Geophysical Research Letters

RESEARCH LETTER
10.1029/2019GL082753

# In Search of Winter Blocking in the Western North Pacific Ocean

**Seon-Hwa Kim**[1] **and Baek-Min Kim**[2]

[1]Korea Polar Research Institute, Incheon, South Korea, [2]Department of Environmental Atmospheric Sciences, Pukyong National University, Busan, South Korea

**Key Points:**
- The western North Pacific blocking events identified by the anomaly type are mostly originated and moved from the eastern North Pacific
- In situ development of the western North Pacific blocking is reasonably captured well by the reversal type
- The two types of detection methods capture unique blocking events that have very different regional surface impacts

**Supporting Information:**
- Supporting Information S1

**Correspondence to:**
B.-M. Kim,
baekmin@pknu.ac.kr

**Citation:**
Kim, S.-H., & Kim, B.-M. (2019). In search of winter blocking in the western North Pacific Ocean. *Geophysical Research Letters*, *46*, 9271–9280. https://doi.org/10.1029/2019GL082753

Received 20 MAR 2019
Accepted 12 MAY 2019
Accepted article online 7 JUN 2019
Published online 13 AUG 2019



**Abstract** We investigate winter blocking activity over the western North Pacific (WNP) through an intercomparison of four detection methods, which are categorized into two types (anomaly and reversal). Most of the blocking events in the anomaly-based methods are initiated from the eastern North Pacific. Reversal-based methods capture the blocking occurrence associated with Rossby wave breaking, especially cyclonic breaking. As the two types capture different aspects of WNP blocking, the resultant regional impact is also largely different. At the onset, anomaly-based methods show a strong cold anomaly downstream of the blocking in conjunction with a Pacific/North America-like pattern. Reversal-based methods indicate a weak cold anomaly in company with a western Pacific-like pattern, which appears downstream and upstream of the blocking in the local reversal and large-scale reversal methods, respectively. At the end of WNP blocking, all methods show strong cold anomalies both upstream and downstream of the blocking.

## 1. Introduction

Atmospheric blocking, which is generally described as a quasi-stationary high-pressure system, interrupts westerly flows and the propagation path of extratropical cyclones through the perturbation of the background flow (Booth et al., 2017; Pelly & Hoskins, 2003). It can lead to extreme weather events such as summer heat waves or winter cold spells (Buehler et al., 2011; Dole et al., 2011; Pfahl, 2014; Trigo et al., 2004). The resulting temperature and precipitation responses vary depending on the location of the blocking (Brunner et al., 2018; Sousa et al., 2017, 2018). Recent studies suggest that warmer Arctic conditions reduce the meridional temperature gradient and weaken jet streams, resulting in increased blocking occurrences (Barnes et al., 2014; Francis & Vavrus, 2012; Hassanzadeh & Kuang, 2015; Kennedy et al., 2016; Kim et al., 2014; Mori et al., 2014). Despite growing recognition of atmospheric blocking's critical impacts, identification is difficult because of the nonuniversal definition of blocking. There are many different atmospheric configurations (e.g., dipole blocks, omega blocks, open ridges, and premature blocks) that consider different fields, so they simply do not recognize the same objects within the atmosphere. Consequently, detection algorithms yield diverse results for blocking occurrence.

The detection methods are generally categorized as either anomaly type (Dole & Gordon, 1983; Sausen et al., 1995) or reversal type (Davini et al., 2012; Masato et al., 2013a; Pelly & Hoskins, 2003; Tibaldi & Molteni, 1990). More recently, a hybrid method (Barriopedro et al., 2010; Dunn-Sigouin et al., 2013) applying the aforementioned two types sequentially has been developed and used in a number of studies (Kim et al., 2017; Kim & Ha, 2015). The three methods show all different blocking climatologies and regional blocking patterns, especially in the western North Pacific (WNP) region. Both the anomaly type and the hybrid type yield higher blocking frequency in the eastern North Pacific (ENP; Barriopedro et al., 2010; Dunn-Sigouin et al., 2013; Kim & Ha, 2015), whereas the reversal type exhibits much higher values of blocking frequency in the WNP (Davini et al., 2012; Masato et al., 2013a). However, an objective comparison among the previous results is a difficult task because each study uses different spatial scales and tracking methodologies, such as different interpretations of overlapping areas and the location of the blocking center for a given domain.

Recent studies have nonetheless attempted to compare several detection methods (Barnes et al., 2014; Barriopedro et al., 2010; Woollings et al., 2018). However, none discussed WNP blocking activity in detail. A few studies have focused on East Asian blocking activity near the WNP region (Lee & Jhun, 2006; Nakamura & Fukamachi, 2004) and analyzed the relationship with large-scale circulation patterns or summertime characteristics. In this study, we conduct an intercomparison of four conventional blocking detection methods with a focus on the blocking activity over the WNP region. Also, inspired by Davini

et al. (2012) and Masato et al. (2013a), we determine which detection methods are suitable for identifying Rossby wave breaking (RWB) associated with blocking development. Finally, the regional temperature impacts are investigated for WNP blocking.

## 2. Data and Methods

### 2.1. Data

This study used data from the daily mean geopotential height at 500 hPa (Z500), with surface air temperature (SAT) derived from the National Center for Environmental Prediction/National Center for Atmospheric Research (NCEP/NCAR) reanalysis (Kalnay et al., 1996) at a resolution of 2.5° × 2.5° for the period of 1950 to 1988. We focus on the winter season from December to March, where the winter of 1950 represents December of 1950 and January to March of 1951. The entire data set covers a total of 4,719 days. An anomaly of a given variable for the composites is calculated with respect to the daily climatology for the period of 1950–1988.

### 2.2. Blocking Detection Methods

We compare the blocking frequencies estimated by four different blocking methods in a two-dimensional latitude-longitude context: one anomaly type, two reversal types, and one hybrid type. In this study, the blocking frequency is defined as the percentage of blocked days per winter season. The first blocking method (hereafter called ANO), which is based on work by Dole and Gordon (1983) and later improved by Sausen et al. (1995), detects blocking occurrence with Z500 anomalies exceeding the predefined anomaly threshold. The second blocking method (hereafter called LOC) searches for a local reversal of the meridional gradient of Z500 at each grid point within the latitude band 50–75°N following work by Davini et al. (2012), which extends Tibaldi and Molteni's (1990) method to two dimensions. The third blocking method is the large-scale reversal method (hereafter called LAR), which finds macroscale reversals of the meridional gradient of Z500 at a central blocking latitude within the band 45–75°N following work by Masato et al. (2013b). The fourth method is the hybrid method (HYB) proposed by Dunn-Sigouin et al. (2013), which identifies blocking only if there exists a local reversal among the blocking events found by the ANO. Since the ANO is first applied in the algorithm sequence, the HYB is a subset of blockings detected by ANO. Thus, the total number of blocking events in the HYB is always less than that in the ANO.

It is worth highlighting that all detection processes are undertaken with the same variable (Z500) and with the same tracking criteria. The Z500 is a widely used variable in blocking detection and works effectively in quasi-barotropic systems. The common tracking criteria are as follows: spatial-scale threshold is $2.5 \times 10^6$ km$^2$, overlap threshold is 50% of the area overlap within 2 days, minimum duration is 5 days, and meridional and zonal scale of the block are both 15°. Our intention here is to apply the same tracking criteria as much as possible so as to obtain objectiveness in the intercomparison of the methods. Amplitude threshold in the anomaly-based methods (HYB and ANO) is set to 1.5 standard deviations of Z500 anomalies over 30°–90°N for a 3-month period centered about a given month. The 3-month period considers seasonal variation in blocking occurrence, following work by Barriopedro et al. (2010; see the supporting information for detailed descriptions of the blocking methods used).

We selected the blocking events where the onset occurs within the December-January-February months. To focus on specific regional blocking, we further restricted the whole life cycle of the blocking events where the blocking center has passed through the WNP region (120°E-180°) at least once. The blocking center is defined as the maximum location of Z500 anomaly around the blocking area. Because blocking centers in the reversal-based methods (LOC and LAR) are not always located within the blocking area, we search for blocking centers by using an expanded blocking area. The longitudinal boundary of the blocking area in the reversal-based methods is extended by 10° on both sides, and the latitudinal boundary of the LOC (LAR) is extended from the minimum (middle) latitude of blocking area to 90°N.

### 2.3. Wave Breaking Index (WBI)

To understand the dynamical process of the blocking development, we investigate the blocking events associated with RWB being part of many theories. We calculate the WBI as Davini et al. (2012) did but with minor modification.

$$\mathrm{WBI}(\lambda_0, \Phi_0) \equiv \frac{Z_{500}(\lambda_W, \Phi_S + 7.5^\circ) - Z_{500}(\lambda_E, \Phi_S + 7.5^\circ)}{\lambda_W - \lambda_E} \quad (1)$$

where $\lambda_0$ and $\Phi_0$ are longitude and latitude of the blocking center, respectively, $\lambda_W = \lambda_0 - 7.5^\circ$, $\lambda_E = \lambda_0 + 7.5^\circ$, and $\Phi_S = \Phi_0 - 15^\circ$.

A reference value of the WBI is increased as follows to more clearly distinguish it

$$\mathrm{WBI} > 5 \rightarrow \text{Cyclonic wave breaking (CB)} \quad (2)$$

$$\mathrm{WBI} < -5 \rightarrow \text{Anticyclonic wave breaking (AB)} \quad (3)$$

We attempted to apply RWB analysis using WBI to all types of blocking detection, which is an extension of the study by Davini et al. (2012) who investigated the WBI detected by LOC. Note that we evaluate the WBI only where the local gradient reversal exists to the south of the blocking center, and all statistics are based on the blocking onset date.

## 3. Results

Figure 1 shows the climatology of winter blocking frequency determined by each detection method. Their geographical distributions show interestingly different patterns. With the anomaly-based methods (Figures 1a and 1b), two principal regions of blocking occurrences are located to the left of the International Date Line. In contrast, the main blocking regions determined by the reversal-based methods (Figures 1c and 1d) are on the right of the International Date Line. In particular, the Atlantic blocking of the reversal-based methods is divided into two maxima. The maxima of the LOC and LAR are over mainland Europe and Greenland, respectively. These results are in good agreement with previous findings (Barnes et al., 2014; Barriopedro et al., 2010; Davini et al., 2012; Dunn-Sigouin et al., 2013; Masato et al., 2013b).

The local maximum blocking frequency of 23.3% among the four methods is from the LAR (Figure 1d) located around the WNP region. Other characteristics for the four methods can be found in the supporting information (Table S1). Although the LAR does not exhibit the highest number of total blocking events and days, both LAR and ANO record the longest blocking duration of 8.9 days. The ANO (LOC) records the highest (lowest) values in terms of both total blocking events and days. From these results, different detection methods evidently produce multifaceted blocking climatologies, which support the argument given by Barriopedro et al. (2010) that the choice of using absolute or anomaly fields to identify blocking phenomena is an important matter.

The colored dots in Figure 1 represent the distribution of WNP blocking center only if the center is located in the WNP region during the whole life cycle of WNP blocking. The centers of anomaly-based methods are relatively widely spread out, but the central region of the distribution is over the central Pacific. On the contrary, the reversal-based methods have a large number of centers on the poleward flank of the Pacific jet stream. The distribution is much more concentrated over the WNP, and the highest number of WNP blocking centers is detected in LAR (see Table S3).

Stationary eddies at 500 hPa, which are simply defined as the zonal mean deviation from the climatological geopotential height field, are also shown by the contours in Figure 1. The blocking frequency maxima of anomaly-based methods are located between the stationary eddies (ridges and troughs), where low-frequency variability is typically strong (Blackmon et al., 1984; Doblas-Reyes et al., 2002). Kushnir (1987) found retrograding (westward moving) features of the low-frequency disturbances over the North Pacific Ocean. A sufficiently strong retrograding signal may modulate the structure of the climatological stationary wave, changing the location of blocking occurrence.

With the reversal-based methods, the WNP blocking matches well with the stationary trough on the poleward side of the jet, whereas the two Atlantic maxima lie on the opposite phase of each eddy. Pelly and Hoskins (2003) were the first to suggest that the onset of the blocking development is associated with the RWB. Since then, many studies have shown that blocking events over WNP are mainly related to CB (Davini et al., 2012; Masato et al., 2013a; Tyrlis & Hoskins, 2008).

Table S2 in the supporting information shows the total number of blocking events where the local gradient reversal exists below the blocking center and the number of events associated with RWB. The differences

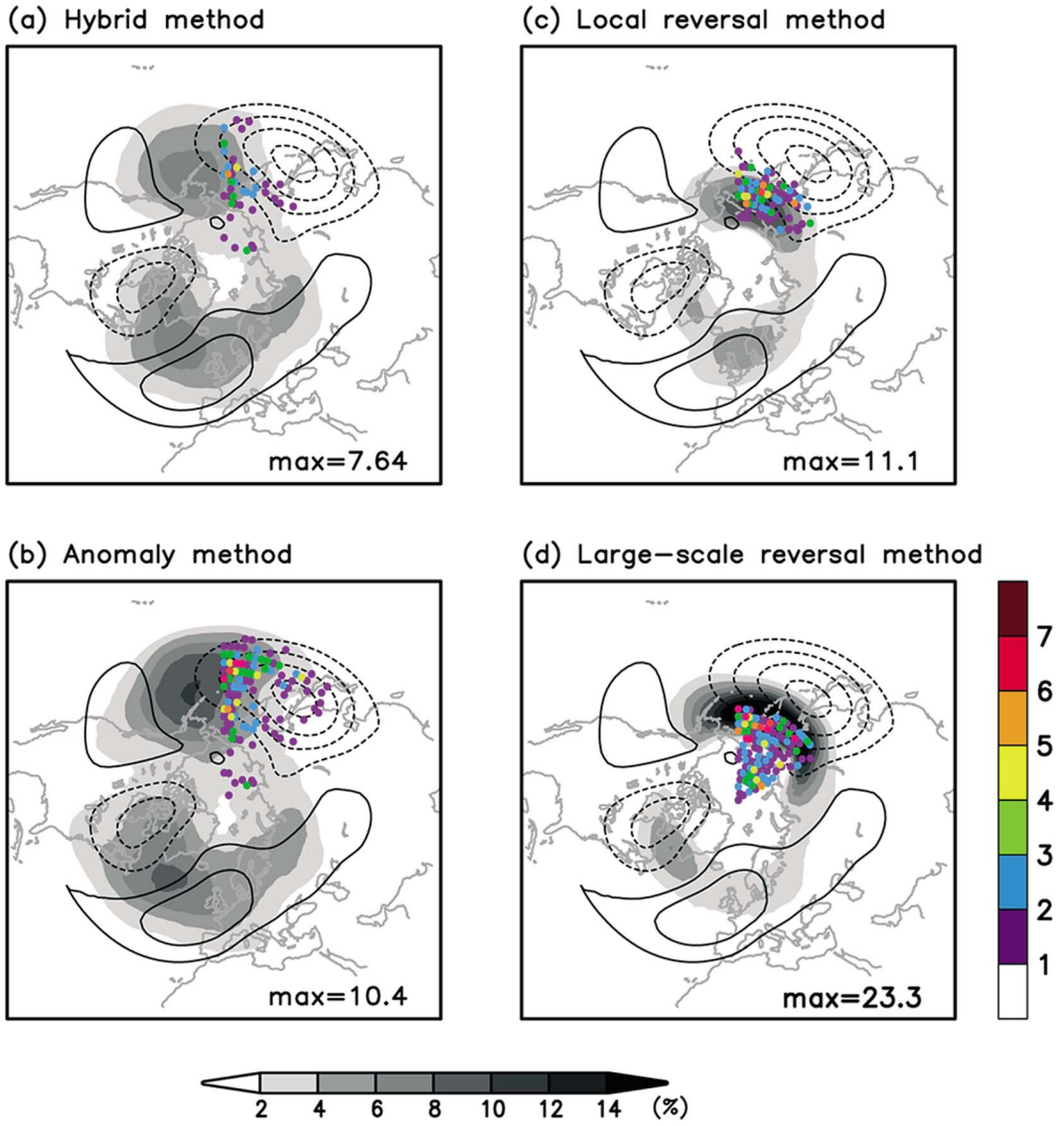


**Figure 1.** Climatology of Northern Hemisphere blocking frequency (gray shading) determined by the (a) HYB, (b) ANO, (c) LOC, and (d) LAR. Units represent the percentage of blocked days per winter (December-January-February-March), with the maximum frequency values indicated at the bottom right of each panel. Contours show climatological stationary eddies at 500 hPa in intervals of 50 m. Colored dots represent the number of occurrences for the positions of blocking centers in the WNP region (120°E-180°).

among the total event number of the four methods are reduced because the total number determined by the anomaly-based methods is strikingly reduced compared to the results shown in Table S1. Anomaly-based methods have the well-known problem of open ridges being activated in the early stages of block development (Barriopedro et al., 2010). Open ridges are reduced because we only consider the cases where easterly winds exist to the south of the blocking center. Regarding the RWB relation, most methods show that the number of blocking events associated with AB is higher than that with CB, except for the LAR.

These features are more clearly distinguished in the spatial distribution map of blocking events associated with RWB determined by each method (Figure 2). In the HYB, the CB and AB events (Figures 2a and 2e) show quite similar blocking event maps compared to other methods. In the ANO, most events over the North Pacific are categorized as CB because AB events rarely exist. Note that the sum of blocking events

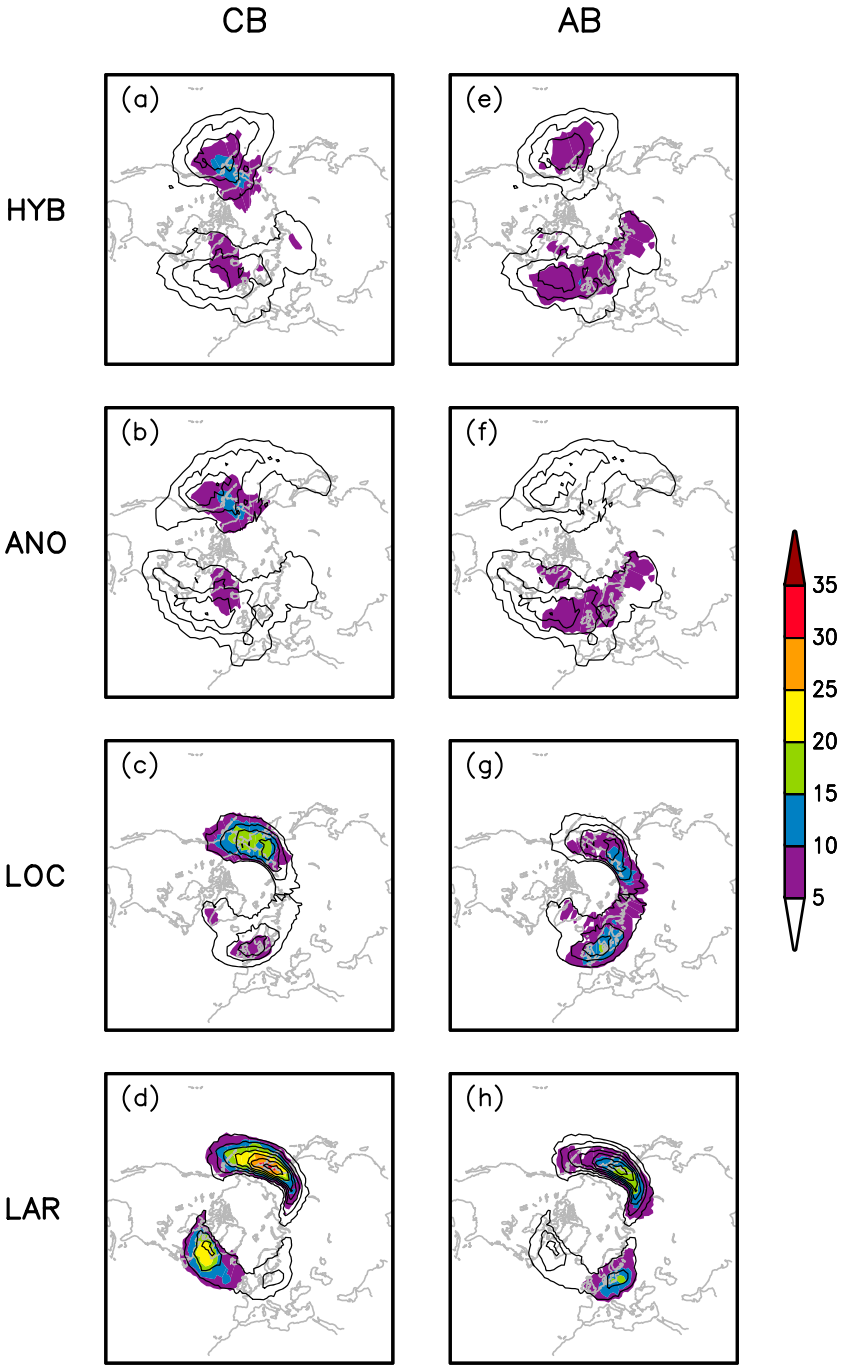


**Figure 2.** Spatial distributions of number of blocking events associated with Rossby wave breaking (shadings) determined by the (a, e) HYB, (b, f) ANO, (c, g) LOC, and (d, h) LAR. Left column and right column show the results for cyclonic wave breaking (CB) and anticyclonic wave breaking (AB), respectively. Contours show total number of blocking events (contours) in intervals of 10.

that belong to CB (Figure 2b) and AB (Figure 2f) of ANO is largely different to the total blocking event map of ANO (contours in Figure 2). Sousa et al. (2018) showed that high-latitude blocking and subtropical ridges occur in different locations, and the temperature responses are completely opposite. Therefore, this result indicates that the events for anomaly-based methods demonstrate the intrinsic problem of open ridges being considered as blocks.

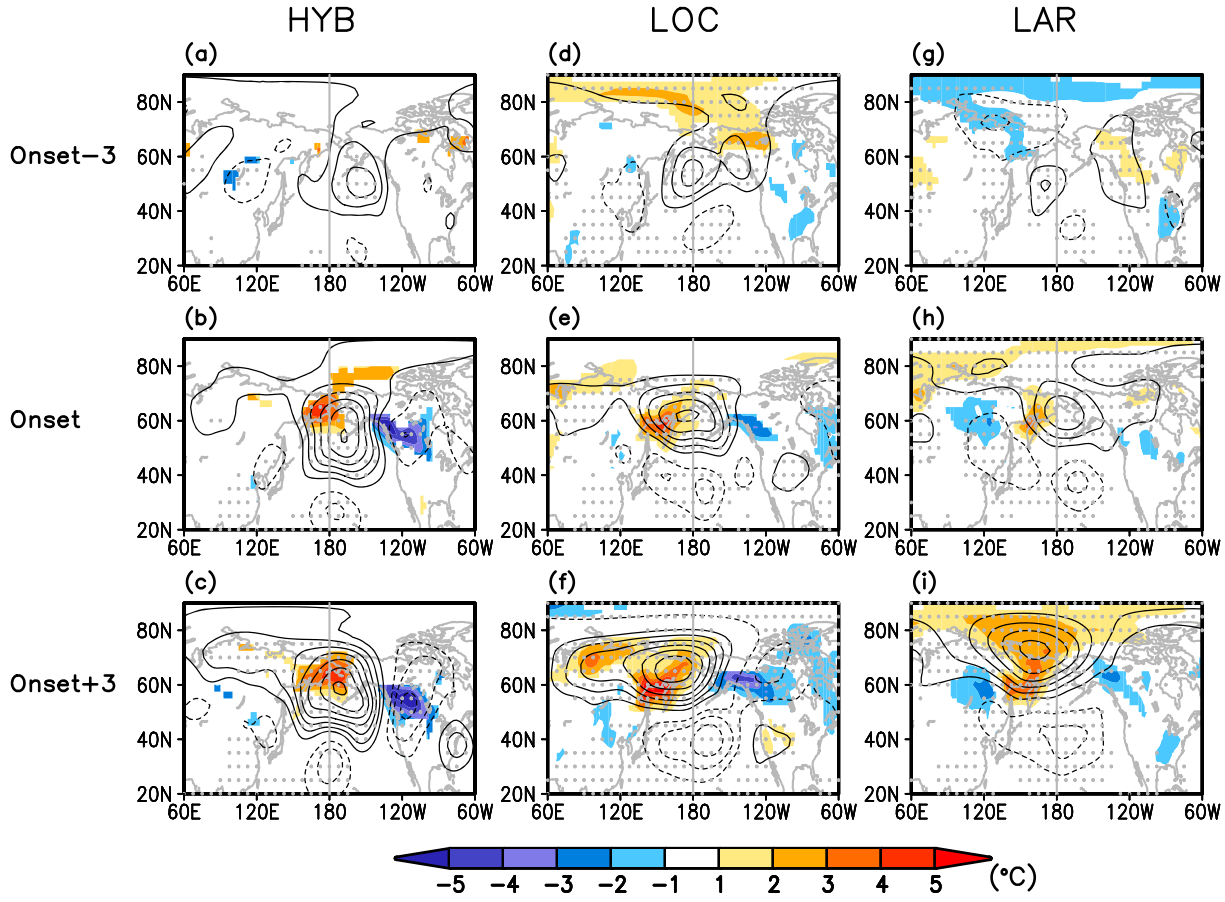


**Figure 3.** Composite evolutions of the WNP (120°E-180°) blocking events shown as a function of the onset time determined by the HYB (a–c), LOC (d–f), and LAR (g–i). Shadings (contours) represent SAT (Z500) anomalies with an interval of 1 °C (20 m). The SAT anomalies that are statistically significant at the 95% confidence level using a two-tailed Student's *t* test are shaded. Stippling indicates regions exceeding 95% confidence level based on the two-tailed Student's *t* test for Z500 anomalies. Gray vertical lines indicate 180° of longitude. The time period spans from 3 days before to 3 days after the onset.

In contrast to the anomaly-based methods, the LOC yields higher values (>15) of CB events around the central North Pacific and WNP regions (Figure 2c). Compared to AB (Figure 2g), CB is an apparently dominant type of RWB in the WNP. LAR is quite similar to LOC, but the CB of LAR produces higher values (>25) over Kamchatka (Figure 2d) than that from LOC. Another difference for the CB of LAR appears in South Greenland, where there is an increased event relative to the CB of LOC (Figure 2c). Note that reversal-based methods show the predominant event of CB in the WNP, which is the location of a climatological trough (contours in Figure 1).

Among the different features, we focus on characteristics of blocking occurrence over the WNP region. (1) Anomaly-based methods do not capture the WNP blocking associated with RWB. (2) WNP blocking occurrence detected by reversal-based methods dominates the CB characteristics. Also, WNP blocking has slightly more blocking days for reversal-based methods than anomaly-based methods, especially in the LAR (Table S3). This is in contrast to the fact that Northern Hemisphere blocking has much more blocking days for anomaly-based methods than reversal-based methods (Table S1). This result suggests the importance of choosing an appropriate threshold for distinct areas in the Northern Hemisphere.

Figure 3 shows the composite evolution of Z500 and SAT anomalies for the onset time of WNP blocking determined by three methods. Because the regional impacts of the ANO are quite similar to those of the HYB, the results of the ANO are excluded for convenience (see Figure S1 in the supporting information for detailed results of the ANO). The total numbers of blocking events in the HYB, LOC, and LAR used for the composite analysis are 62, 75, and 111, respectively (Table S3). Three days before the onset, a positive Z500 anomaly of the HYB is pronounced over the ENP, where the low-frequency eddy is strong. The positive

Z500 anomaly becomes stronger over time and moves westward, which is also found in the ANO (Figure S1). This result indicates that the WNP blocking occurrence in the anomaly-based methods may be related to the retrograding signal of low-frequency eddy. Reversal-based methods show distinct positive anomalies over the central Pacific, although a positive Z500 anomaly of the LAR is small scale. At the onset, the HYB (Figure 3b) indicates both a meridional dipolar structure of Z500 anomalies over the central Pacific and negative Z500 anomalies over western America. This distribution resembles the Pacific/North America (PNA) teleconnection pattern (Wallace & Gutzler, 1981) and becomes more similar after 3 days (Figure 3c). Reversal-based methods (Figures 3e and 3h) show a noticeable dipolar structure of Z500 anomalies around the central Pacific, including the strong positive and negative height anomalies at middle latitude and low latitude, respectively. These dipolar structures become stronger with time, increasing the similarity with the western Pacific (WP) pattern (Wallace & Gutzler, 1981). Woollings et al. (2008) suggested that the negative phase of the WP pattern occurs in association with WNP blocking derived from the LAR. The LOC (Figure 3f) also reveals a negative Z500 anomaly in western America, which is broadly distributed in merging with the negative anomaly in the Pacific Ocean. The reversal-based methods after 3 days (Figures 3f and 3i) represent a slightly westward-tilted dipolar structure as the center of blocking anticyclone moves to the WNP. It is also interesting that the latitude range in the spatial scale of the blocking anticyclone between the LOC and LAR is different. The LOC has a closed anticyclonic circulation ranging from 55°N to 80°N, whereas the anticyclonic circulation of the LAR ranges from 60°N to 90°N. These differences result from the different latitude criteria (i.e., central latitude or central blocking latitude) in the detection algorithm.

In view of the SAT anomaly, LOC and LAR 3 days before the onset (Figures 3d and 3g) exhibit warm and cold anomalies on the poleward flank of anticyclone over the central Pacific and cyclone over the Laptev Sea, respectively. Because midtropospheric blocking has an equivalent barotropic structure (Davini et al., 2012), all methods at the onset (Figures 3b, 3e, and 3h) show robust warm anomalies on the western side of WNP blocking. HYB and LOC have distinct cold anomalies downstream of WNP blocking, but the LAR has a cold anomaly upstream of WNP blocking. Three days from the onset, this distribution becomes much stronger than before and the LAR (Figure 3i) also shows cold anomalies both upstream and downstream of the WNP blocking.

Figure 4 shows the composite evolution for the end time of WNP blocking, and an associated downstream development occurs in various ways for each detection method (see Figure S2 for details). Three days before the end, the overall distribution of Z500 anomalies for all three methods (Figures 4a, 4d, and 4g) is greatly intensified, showing a typical mature stage of block development. The difference from the previous one is that the negative Z500 anomalies of the LOC exist widely in the Arctic and North America, and the LAR represents the negative anomalies in the central Pacific extending to western America. During the end time of the HYB (Figure 4b), a zonally symmetric pattern is remarkable. Reversal-based methods (Figures 4e and 4h) exhibit a westward-titled wave train pattern because of cyclonic anomalies merging between low latitude and the Arctic and anticyclonic anomalies over southwestern North America. Three days after the end, the WNP blocking anticyclone is much reduced in all methods (Figures 4c, 4f, and 4i). A pronounced negative Z500 anomaly exists widely in Alaska, and a positive Z500 anomaly still appears in southwestern North America. It is evident in all methods that the center of WNP blocking moves in a westward direction over time. This result is consistent with the findings of Carrera et al. (2004), who found that most of the ENP blockings derived from the ANO move westward and disappear in the WNP.

With regard to the near-surface level, a strong warm anomaly in all methods (Figures 4a, 4d, and 4g) is observed widely around WNP blocking anticyclone 3 days before the end. A strong cold anomaly in all methods also appears on the downstream side near western America, especially in the HYB. The LOC shows strong cold anomalies in eastern America as well as in the Arctic, which seems to be related to widespread cyclonic circulation to the Arctic. At the upstream of the WNP blocking, cold anomalies appear in two methods. The HYB is very strong in the latitude range of 50–60°N, while the LAR shows substantial cold anomaly in the latitude range of 55–65°N. This SAT distribution continues to be strong at the end of WNP blocking (Figures 4b, 4e, and 4h). As the WNP blocking anticyclone moves westward, the warm anomalies shift westward as a whole. Cold anomalies over northwest America move slightly westward in the same manner and are much wider and stronger than before. In all methods, as the blocking anticyclone moves to the southwest, the cold anomaly over East Asia becomes stronger with southward expansion. Three days after the

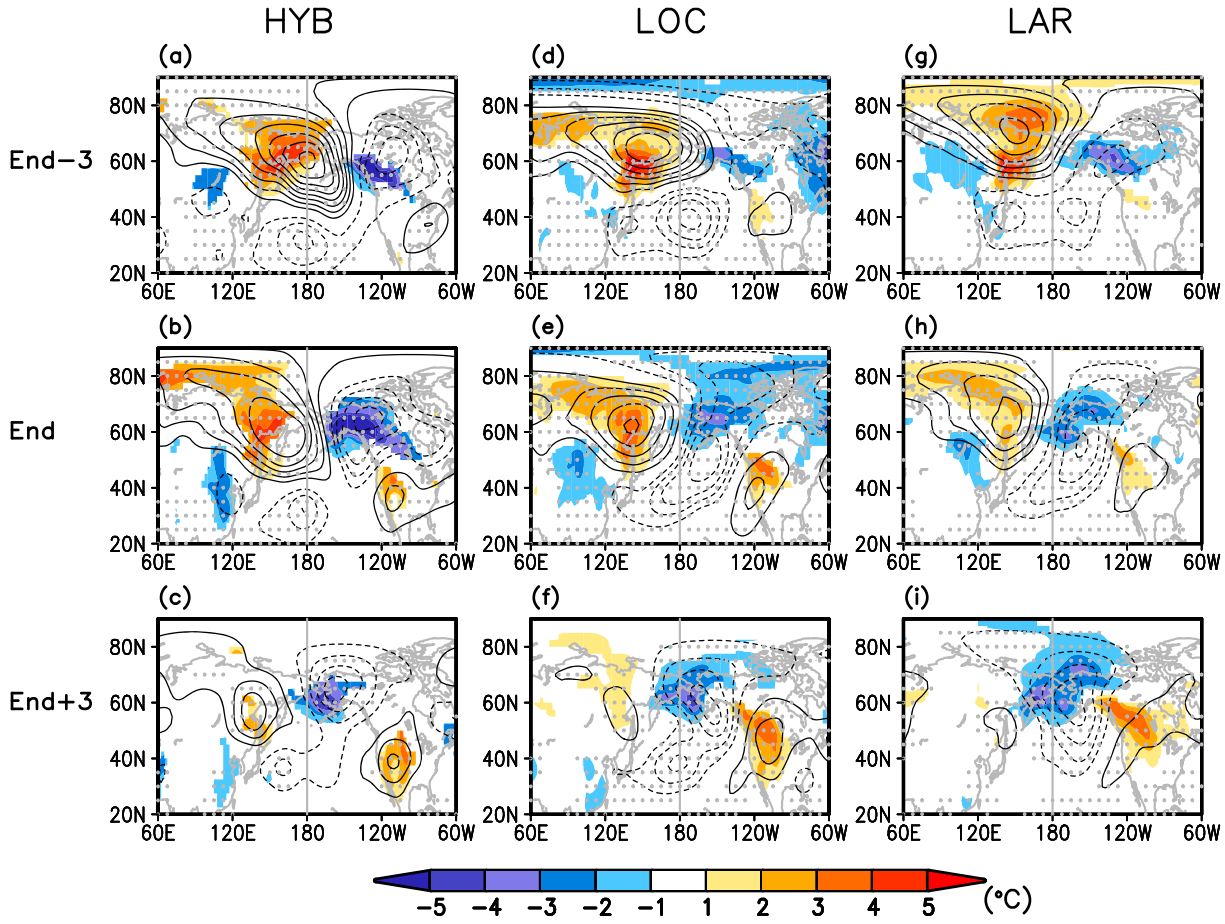


**Figure 4.** As in Figure 3 but for the end time of western North Pacific blocking events.

end (Figures 4c, 4f, and 4i), the warm anomalies around the WNP blocking almost disappear and strong cold anomalies persist, centered over Alaska. In the southwestern North America, warm anomalies are consistently strong from the end of WNP blocking.

## 4. Summary and Discussion

This study investigates the two-dimensional distribution of WNP blocking frequency among different blocking detection methods under the same detection tracking criteria. The resultant blocking frequency maps are largely different depending on whether anomaly or reversal-type methods are initially applied. In the Pacific region, anomaly- and reversal-based methods show higher blocking frequencies in the ENP and WNP, respectively. In the Atlantic, the main location of the blocking frequency detected by reversal-based methods is slightly different with the preferred location (e.g., central Atlantic) of anomaly-based methods but not that large compared to the Pacific case.

Focusing on the WNP region, it is revealed that the anomaly- and reversal-based methods essentially differ in capturing the major mechanisms of the WNP blocking development. Most of the WNP blockings detected in the anomaly-based methods originate from blocking occurrence in the ENP. The westward retrograding of strong low-frequency eddies from the ENP induces ridge amplification, eventually increasing the blocking occurrences in the WNP. On the other hand, reversal-based methods capture the in situ blocking occurrence in the WNP with the RWB process. CB is preferred to AB in the blocking initiation, and this can be related to the preexisting stationary trough in the WNP.

From the onset of WNP blocking, regional impacts determined by each detection method have changed dramatically on a daily basis. Anomaly-based methods during the blocking onset show a strong cold anomaly

downstream of the blocking in conjunction with a PNA-like pattern. On the other hand, the reversal-based methods represent a weak but distinct cold anomaly. The cold anomaly in the LOC and LAR appears downstream and upstream of the blocking, respectively. The midtropospheric distribution also shows a WP-like pattern, but there is a slight difference that the positive Z500 anomalies of the LAR cover the Arctic. At the end of the WNP blocking period, strong cold anomalies exist both upstream and downstream of the blocking in all detection methods. In the distribution of the Z500 anomaly, the anomaly-based methods show a zonally symmetric pattern and the reversal-based methods show a westward-titled wave train. After the end of WNP blocking, a strong cold anomaly has persisted for a long time, which is accompanied by a cyclonic circulation around Alaska.

As discussed by Barriopedro et al. (2010) and Dunn-Sigouin et al. (2013), anomaly-based methods suffer from the effects of open ridges and subtropical highs, and reversal-based methods suffer from cutoff lows and missing immature blocks. We found that the LAR incorrectly detects planetary-scale high pressures (not shown). The HYB is also designed to overcome the weakness of both anomaly-based and reversal-based methods, but the results are more similar to the anomaly-based methods, and above all, it does not seem to count the blocking events originating from wave breaking properly. It is rather surprising that regional blocking events are so sensitive to the detection methods. Considering these problems, further efforts toward the development of a unified blocking detection algorithm are required.

**Acknowledgments**
The NCEP/NCAR reanalysis data can be provided by the NOAA/OAR/ESRL PSD, Boulder, Colorado, USA, from their Web site (http://www.esrl.noaa.gov/psd/). This work was supported by "Investigation and Prediction system development of Marine Heatwave around the Korean Peninsula originated from the Sub-Arctic and Western Pacific" project (KOPRI, 20190344), funded by the Ministry of Oceans and Fisheries, Korea.

## References

Barnes, E. A., Dunn-Sigouin, E., Masato, G., & Woollings, T. (2014). Exploring recent trends in Northern Hemisphere blocking. *Geophysical Research Letters*, *41*, 638–644. https://doi.org/10.1002/2013GL058745

Barriopedro, D., García-Herrera, R., & Trigo, R. M. (2010). Application of blocking diagnosis methods to general circulation models. Part I: A novel detection scheme. *Climate Dynamics*, *35*(7-8), 1373–1391. https://doi.org/10.1007/s00382-010-0767-5

Blackmon, M. L., Lee, Y. H., & Wallace, J. M. (1984). Horizontal structure of 500 mb height fluctuations with long, intermediate and short time scales. *Journal of the Atmospheric Sciences*, *41*(6), 961–980. https://doi.org/10.1175/1520-0469(1984)041<0961:HSOMHF>2.0.CO;2

Booth, J. F., Dunn-Sigouin, E., & Pfahl, S. (2017). The relationship between extratropical cyclone steering and blocking along the North American East coast. *Geophysical Research Letters*, *44*, 11,976–11,984. https://doi.org/10.1002/2017GL075941

Brunner, L., Schaller, N., Anstey, J., Sillmann, J., & Steiner, A. K. (2018). Dependence of present and future European temperature extremes on the location of atmospheric blocking. *Geophysical Research Letters*, *45*, 6311–6320. https://doi.org/10.1029/2018GL077837

Buehler, T., Raible, C. C., & Stocker, T. F. (2011). The relationship of winter season North Atlantic blocking frequencies to extreme cold or dry spells in the ERA-40. *Tellus A*, *63*(2), 174–187. https://doi.org/10.1111/j.1600-0870.2010.00492.x

Carrera, M. L., Higgins, R. W., & Kousky, V. E. (2004). Downstream weather impacts associated with atmospheric blocking over the northeast Pacific. *Journal of Climate*, *17*(24), 4823–4839. https://doi.org/10.1175/JCLI-3237.1

Davini, P., Cagnazzo, C., Gualdi, S., & Navarra, A. (2012). Bidimensional diagnostics, variability and trends of Northern Hemisphere blocking. *Journal of Climate*, *25*(19), 6496–6509. https://doi.org/10.1175/JCLI-D-12-00032.1

Doblas-Reyes, F. J., Casado, M. J., & Pastor, M. A. (2002). Sensitivity of the Northern Hemisphere blocking frequency to the detection index. *Journal of Geophysical Research*, *107*(D2), 4009. https://doi.org/10.1029/2000JD000290

Dole, R., Hoerling, M., Perlwitz, J., Eischeid, J., Pegion, P., Zhang, T., et al. (2011). Was there a basis for anticipating the 2010 Russian heat wave? *Geophysical Research Letters*, *38*, L06702. https://doi.org/10.1029/2010GL046582

Dole, R. M., & Gordon, N. D. (1983). Persistent anomalies of the extratropical Northern Hemisphere wintertime circulation: Geographical distribution and regional persistence characteristics. *Monthly Weather Review*, *111*(8), 1567–1586. https://doi.org/10.1175/1520-0493(1983)111<1567:PAOTEN>2.0.CO;2

Dunn-Sigouin, E., Son, S., & Lin, H. (2013). Evaluation of Northern Hemisphere blocking climatology in the global environment multiscale model. *Monthly Weather Review*, *141*(2), 707–727. https://doi.org/10.1175/MWR-D-12-00134.1

Francis, J. A., & Vavrus, S. J. (2012). Evidence linking Arctic amplification to extreme weather in mid-latitudes. *Geophysical Research Letters*, *39*, L06801. https://doi.org/10.1029/2012GL051000

Hassanzadeh, P., & Kuang, Z. (2015). Blocking variability: Arctic Amplification versus Arctic Oscillation. *Geophysical Research Letters*, *42*, 8586–8595. https://doi.org/10.1002/2015GL065923

Kalnay, E., Kanamitsu, M., Kistler, R., Collins, W., Deaven, D., Gandin, L., et al. (1996). The NCEP/NCAR 40 year reanalysis project. *Bulletin of the American Meteorological Society*, *77*(3), 437–471. https://doi.org/10.1175/1520-0477(1996)077<0437:TNYRP>2.0.CO;2

Kennedy, D., Parker, T., Woollings, T., Harvey, B., & Shaffrey, L. (2016). The response of high-impact blocking weather systems to climate change. *Geophysical Research Letters*, *43*, 7250–7258. https://doi.org/10.1002/2016GL069725

Kim, B. M., Hong, J. Y., Jun, S. Y., Zhang, X., Kwon, H., Kim, S. J., et al. (2017). Major cause of unprecedented Arctic warming in January 2016: Critical role of an Atlantic windstorm. *Scientific Reports*, *7*(1), 40051. https://doi.org/10.1038/srep40051

Kim, B. M., Son, S. W., Min, S. K., Jeong, J. H., Kim, S. J., Zhang, X., et al. (2014). Weakening of the stratospheric polar vortex by Arctic sea-ice loss. *Nature Communications*, *5*(1), 4646. https://doi.org/10.1038/ncomms5646

Kim, S. H., & Ha, K. J. (2015). Two leading modes of Northern Hemisphere blocking variability in the boreal wintertime and their relationship with teleconnection patterns. *Climate Dynamics*, *44*(9-10), 2479–2491. https://doi.org/10.1007/s00382-014-2304-4

Kushnir, Y. (1987). Retrograding wintertime low-frequency disturbances over the North Pacific Ocean. *Journal of the Atmospheric Sciences*, *44*(19), 2727–2742. https://doi.org/10.1175/1520-0469(1987)044<2727:RWLFDO>2.0.CO;2

Lee, H. S., & Jhun, J. G. (2006). Two types of the Asian continental blocking and their relation to the east Asian monsoon during the boreal winter. *Geophysical Research Letters*, *33*, L22707. https://doi.org/10.1029/2006GL027948

Masato, G., Hoskins, B. J., & Woollings, T. (2013a). Wave-breaking characteristics of Northern Hemisphere winter blocking: A two-dimensional approach. *Journal of Climate*, *26*(13), 4535–4549. https://doi.org/10.1175/JCLI-D-12-00240.1

Masato, G., Hoskins, B. J., & Woollings, T. (2013b). Winter and summer Northern Hemisphere blocking in CMIP5 models. *Journal of Climate*, *26*(18), 7044–7059. https://doi.org/10.1175/JCLI-D-12-00466.1

Mori, M., Watanabe, M., Shiogama, H., Inoue, J., & Kimoto, M. (2014). Robust Arctic sea-ice influence on the frequent Eurasian cold winters in past decades. *Nature Geoscience*, *7*(12), 869–873. https://doi.org/10.1038/ngeo2277

Nakamura, H., & Fukamachi, T. (2004). Evolution and dynamics of summertime blocking over the Far East and the associated surface Okhotsk high. *Quarterly Journal of the Royal Meteorological Society*, *130*(599), 1213–1233. https://doi.org/10.1256/qj.03.101

Pelly, J. L., & Hoskins, B. J. (2003). A new perspective on blocking. *Journal of the Atmospheric Sciences*, *60*(5), 743–755. https://doi.org/10.1175/1520-0469(2003)060<0743:ANPOB>2.0.CO;2

Pfahl, S. (2014). Characterising the relationship between weather extremes in Europe and synoptic circulation features. *Natural Hazards and Earth System Sciences*, *14*(6), 1461–1475. https://doi.org/10.5194/nhess-14-1461-2014

Sausen, R., König, W., & Sielmann, F. (1995). Analysis of blocking events from observations and ECHAM model simulations. *Tellus A*, *47*(4), 421–438. https://doi.org/10.1034/j.1600-0870.1995.t01-3-00003.x

Sousa, P. M., Trigo, R. M., Barriopedro, D., Soares, P. M., Ramos, A. M., & Liberato, M. L. (2017). Responses of European precipitation distributions and regimes to different blocking locations. *Climate Dynamics*, *48*(3-4), 1141–1160. https://doi.org/10.1007/s00382-016-3132-5

Sousa, P. M., Trigo, R. M., Barriopedro, D., Soares, P. M., & Santos, J. A. (2018). European temperature responses to blocking and ridge regional patterns. *Climate Dynamics*, *50*(1-2), 457–477. https://doi.org/10.1007/s00382-017-3620-2

Tibaldi, S., & Molteni, F. (1990). On the operational predictability of blocking. *Tellus A*, *42*(3), 343–365. https://doi.org/10.1034/j.1600-0870.1990.t01-2-00003.x

Trigo, R. M., Trigo, I. F., DaCamara, C. C., & Osborn, T. J. (2004). Climate impact of the European winter blocking episodes from the NCEP/NCAR Reanalyses. *Climate Dynamics*, *23*(1), 17–28. https://doi.org/10.1007/s00382-004-0410-4

Tyrlis, E., & Hoskins, B. J. (2008). The morphology of Northern Hemisphere blocking. *Journal of the Atmospheric Sciences*, *65*(5), 1653–1665 . https://doi.org/10.1175/2007JAS2338.1

Wallace, J. M., & Gutzler, D. S. (1981). Teleconnections in the geopotential height field during the Northern Hemisphere winter. *Monthly Weather Review*, *109*(4), 784–812. https://doi.org/10.1175/1520-0493(1981)109<0784:TITGHF>2.0.CO;2

Woollings, T., Barriopedro, D., Methven, J., Son, S. W., Martius, O., Harvey, B., et al. (2018). Blocking and its response to climate change. *Current Climate Change Reports*, *4*(3), 287–300. https://doi.org/10.1007/s40641-018-0108-z

Woollings, T., Hoskins, B., Blackburn, M., & Berrisford, P. (2008). A new Rossby wave-breaking interpretation of the North Atlantic Oscillation. *Journal of the Atmospheric Sciences*, *65*(2), 609–626. https://doi.org/10.1175/2007JAS2347.1